Polarization anisotropy in quasiplanar sidewall quantum wires on patterned GaAs (311)A substrates

Paulo V. Santos,[a] R. Nötzel, and K. H. Ploog
Paul-Drude-Institut für Festkörperelektronik, Hausvogteiplatz 5-7, D-10117 Germany

(Received 22 December 1998; accepted for publication 9 March 1999)

The polarization anisotropy of the photoluminescence from quasiplanar quantum wires fabricated on the sidewall of $[0\bar{1}1]$-oriented mesas on the (311)A GaAs surface is investigated using a modulation technique that combines high spatial ($\sim 1\ \mu$m) and polarization resolution ($<0.1\%$). Due to their low symmetry, (311)A-oriented quantum wells are intrinsically anisotropic with the fundamental transition preferentially oriented along the $[\bar{2}33]$ direction. The anisotropy contribution from the lateral confinement in the $[0\bar{1}1]$ wires opposes that from the vertical confinement. With increasing lateral confinement, the wire anisotropy initially reduces and then changes its sign. The lateral extent of the electronic wave functions involved in the anisotropic transitions is obtained from a comparison of the results with a theoretical model. © *1999 American Institute of Physics.* [S0021-8979(99)07012-7]

I. INTRODUCTION

The lateral confinement of carriers in semiconductor quantum wires (QWRs) provides an additional degree of freedom for the control of the materials electronic properties to those found in conventional quantum well (QW) structures. Different technological schemes have been used in the past to fabricate QWR structures: most prominent are the (cleaved) edge overgrowth method[1] and the formation of wires on V grooves patterned in (100) GaAs.[2] These structures, however, are highly nonplanar, hindering severely their integration with conventional planar device structures.

Recently, an alternative approach for the fabrication of quasiplanar low-dimensional structures has been introduced based on the growth of a QW on the sidewalls of shallow mesas (10–15 nm high) patterned on (311)A GaAs surfaces.[3,4] The structure of these wires is illustrated schematically in Fig. 1. The growth mode on the patterned (311) surface forms a fast growing mesa sidewall bound by a convex unfaceted surface profile that leads to a quasiplanar lateral quantum wire in a GaAs/(AlGa)As heterostructure. The thicknesses d_z of the wires are typically twice as large as that of the surrounding QW and their widths d_x lie between 40 and 50 nm. The wires exhibit narrow luminescence lines[5] and high cross sections for the capture of carriers from the surrounding QW.[6,7]

An interesting question regarding the sidewall wires is whether the lateral confinement in these structures is sufficiently strong to induce quantum confinement effects. The lateral confinement of the electron wave function has been proven by magneto-photoluminescence spectroscopy[5] and by the observation of one-dimensional subbands in photoluminescence excitation experiments using near field optics.[6] In this contribution, we address the influence of the lateral confinement on the polarization of the QWR photoluminescence. In a truly one-dimensional system, charge carriers can only oscillate and emit radiation along the wire direction, thus making their PL polarized. As observed for other QWR structures,[8–12] we will demonstrate that the PL from sidewall QWRs becomes indeed polarized along the wire axis, due to the existence of lateral quantum confinement. A special feature of the sidewall structures is that due to their quasiplanar arrangement, the polarization properties are less affected by geometric effects such as lateral refractive index modulations as in nonplanar structures.[12] As a result, the lateral confinement dimension d_x can be precisely determined from the amplitude of the anisotropy. In addition, the anisotropy introduced by the lateral confinement (i.e., along $x=[\bar{2}33]$) in the sidewall QWR opposes the intrinsic anisotropy of (311)-oriented QWs. As a consequence, the preferential polarization direction changes from $[\bar{2}33]$ to $[0\bar{1}1]$ with increasing lateral confinement. This inversion, while allowing a detailed investigation of the relative roles of the lateral and vertical confinement on the band structure, offers a new degree of freedom for the design of polarization-controlled optical devices.

This article is organized as follows. We start in Sec. II with a discussion of the anisotropy mechanisms in the wires based on the tight-binding and on the $\mathbf{k}\cdot\mathbf{p}$ approach. This section will provide the necessary background for the quantitative interpretation of the experimental results. Section III describes the structure of the samples and the experimental procedure to measure the photoluminescence anisotropy. Due to the relatively small PL anisotropies and the requirement of high spatial resolution, a modulation technique was employed, which combines confocal microscopy with the use of a photoelastic modulator and multichannel detection.

[a]Author to whom correspondence should be addressed; electronic mail: santos@pdi-berlin.de.

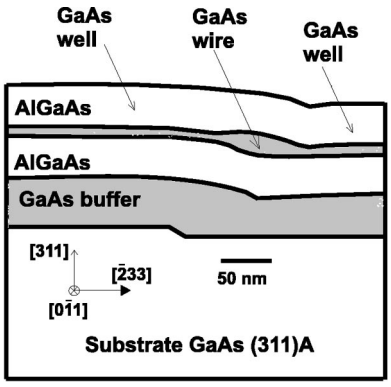

FIG. 1. Structure of sidewall quantum wires on patterned (311)A GaAs substrates.

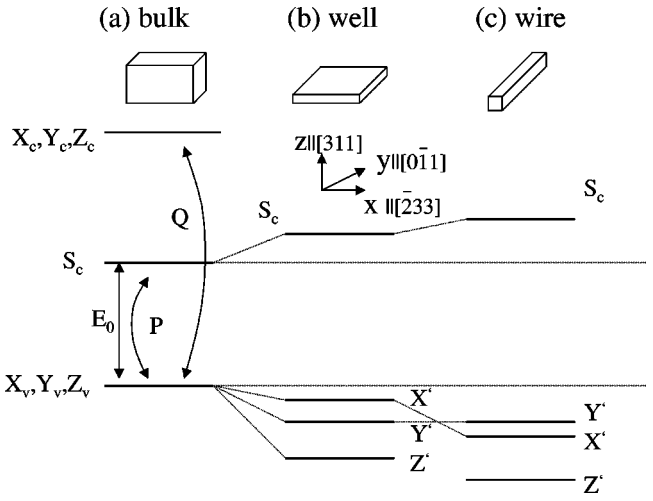

FIG. 2. Relative position of the band edge states in (a) bulk GaAs, (b) (311)-oriented GaAs QW, and (c) in a GaAs QWR with confinement along the $z'=[311]$ and $x'=[\bar{2}33]$ directions. The effects of the spin-orbit coupling are not taken into account.

The experimental results, summarized in Sec. IV, are then compared with the theoretical predictions in Sec. V. Section VI summarizes the main conclusions of this work.

II. OPTICAL ANISOTROPY OF (311)-ORIENTED QUANTUM WIRES

The optical anisotropy near the fundamental band gap arises from the mixing of the p-like valence band states induced by the confinement. If the confinement potentials are large, the eigenstates of the QWR correspond to those of the bulk material with wave vectors along z and x equal to multiples of $k_z=\pi/d_z$ and $k_x=\pi/d_x$, respectively. These eigenstates can be obtained in the effective mass approximation by applying the $\mathbf{k}\cdot\mathbf{p}$-perturbation method to calculate the bulk wave functions away from the Γ point.[13] We shall follow here an alternative procedure based on a combination of the $\mathbf{k}\cdot\mathbf{p}$ with the tight-binding method. This procedure provides a better insight into the mechanisms responsible for the anisotropy. In addition, it can be easily extended to account for confinement effects along other crystallographic axes on $(n11)$-oriented structures.

We start (see Fig. 2) with a basis consisting of one s-like orbital (S_c) to describe the conduction band and three p-like orbitals X, Y, and Z oriented along the main crystallographic axes $[\bar{2}33]$, $[0\bar{1}1]$, and $[311]$, respectively. Linear combinations of the p-like orbitals form the highest valence [Γ_{4v}, corresponding to states X_v, Y_v, Z_v in Fig. 2(a)] and the second lowest conduction bands (Γ_{4c}, states X_c, Y_c, Z_c) at the Γ point. Neglecting at first the spin-orbit interaction, the coupling between these bands, which is induced by the vertical confinement wave vector k_z in a QW, can be described by the $\mathbf{k}\cdot\mathbf{p}$ matrix elements P and Q.[14] The first contribution to the coupling, which is proportional to $|P|^2$ and described in the following by a Hamiltonian $H_{pp,c}$, is the strongest: it mixes the Z_v valence band with the s-like conduction band and lifts the degeneracy between the Z_v and the X_v and Y_v states. The second contribution, denoted $H_{pp,m}$, couples the Γ_{4v} and Γ_{4c} bands through Q and leads to an interaction between the X_v and Z_v states. Interestingly, neither of the contributions mix the p_y-like orbitals with p_x or p_z. As a consequence, the eigenstates X' and Z' become linear combinations of the original X_v and Z_v orbitals (without Y_v components). The effective repulsion between the X_v and Z_v states lifts the degeneracy between the X_v and Y_v bands. The second contribution is responsible for the in-plane optical anisotropy of (311)-oriented QWs. Note that the PL due to the lowest energy transition ($X_v\rightarrow S_c$) is expected to be preferentially polarized along the $x=[\bar{2}33]$ direction.

The effects of the lateral confinement [along x, cf. Fig. 2(c)] on the valence states can be taken into account in a first approximation by including only the coupling to the S_c band induced by the in-plane wave vector k_x (the interaction with the Γ_4 conduction band is neglected in this approximation). A sufficiently large k_x shifts the energy of the X' states below that of the Y' state, thus leading to a change in sign of the in-plane anisotropy of the QWR relative to that of the (311) QW.

An analytical expression for the effective Hamiltonian $H_{pp}=H_{pp,c}+H_{pp,m}$ describing the interaction between the valence band states in the presence of confinement along all three crystallographic directions for a $(n11)$-oriented structure can be obtained using a tight-binding approach. The p-like orbitals X_v, Y_v, and Z_v are chosen to be aligned with the main axes $[\bar{2}nn]$, $[0\bar{1}1]$, and $[n11]$, respectively. Details of the derivation will be described elsewhere.[15] For the case of a confinement along the $z\|[n11]$ and $x\|[\bar{2}nn]$ directions with a confinement dimension ratio $r_t=d_z/d_x\ll 1$, the following expression for H_{pp} (in the basis $\{X_v,Y_v,Z_v\}$) is obtained:[15]

$$H_{pp}=-\frac{1}{2m_0}k_z^2\left[\frac{1}{m_{\mathrm{hh}}^*}\mathbf{1}+H_{pp,c}+H_{pp,m}\right],$$

$$H_{pp,c}=6\gamma_2\begin{bmatrix} r_t^2 & 0 & 0\\ 0 & 0 & 0\\ 0 & 0 & 1\end{bmatrix},$$

$$H_{pp,m}=\frac{1}{m^*_{\rm hh}}\frac{v}{v+1}\begin{bmatrix} 3\sin^2\chi\cos^2\chi & 0 & (\frac{3}{2}\cos^2\chi-1)\sin^2\chi \\ 0 & \cos^2\chi & 0 \\ (\frac{3}{2}\cos^2\chi-1)\sin^2\chi & 0 & -\cos^2\chi(1+3\sin^2\chi) \end{bmatrix}. \quad (2.1)$$

Here, m_0 and $m^*_{\rm hh}$ are the free-electron and the effective heavy-hole masses, respectively, γ_2 is a Luttinger parameter, and $v=V_{xy}/V_{xx}=(V_{pp\sigma}-V_{pp\pi})/(2V_{pp\sigma}+V_{pp\pi})$ is a ratio between tight-binding parameters for the GaAs bond.[16] χ is the angle between the z axis and the [011] direction ($\chi=\sin^{-1}(3/\sqrt{11})$ for (311)-oriented structures). The model assumes infinite confinement barriers and a dimension ratio $r_t=d_z/d_x\ll 1$. The terms $H_{pp,c}$ and $H_{pp,m}$ have cylindrical and orthorhombic symmetries, respectively, and arise from the interaction of the Γ_4 valence states with the S_c and the Γ_{4c} conduction bands. In the calculations to be presented below, the following parameter values were used: $m^*_{\rm hh}=0.41$, $\gamma_2=2.1$, and $v=0.67$.[17]

The interaction between the Γ_{4v} states in Eq. (2.1) leads to a coupling between the heavy (hh), light (lh), and the spin-orbit split (so) hole states, when the spin-orbit coupling is included. This interaction can be obtained in a straightforward way by transforming H_{pp} from the $\{X_v,Y_v,Z_v\}$ basis to the {hh,lh,so} basis and diagonalizing the resulting 3×3 Hamiltonian. The dipole transition matrix elements M between the valence and conduction band states follow directly from the wave functions. Although the so-coupling mixes the X_v and Y_v p states, the preferential polarization of the electron(e)-hh and e-lh transitions remains equal to that of the $e-X_v$ and $e-Y_v$ transitions.

The procedure described above was used to calculate the in-plane anisotropy δ of the squared dipole matrix elements $|M|^2$ for the e-hh and for the e-lh transition in (311)-oriented QWR as a function of the wire thickness and width. The anisotropy is defined as

$$\delta=2\frac{|M_{[\bar{2}33]}|^2-|M_{[0\bar{1}1]}|^2}{|M_{[\bar{2}33]}|^2+|M_{[0\bar{1}1]}|^2}, \quad (2.2)$$

so that it is positive for the e-hh transition in (311)QWs. The dependence of the anisotropy on the well thickness is summarized in Fig. 3(a). In the case of quantum wells (filled symbols), the results based on Eq. (2.1) (squares) compare well with calculations based on the solution of the 6×6 Luttinger Hamiltonian (triangles, from Ref. 13). The anisotropy is approximately constant for well thicknesses above $d_z\sim 6$ nm and increases for narrower wells. The latter effect is attributed to the increasing interaction between the hh and the spin-orbit split hole band for narrower QWs.[18]

The effects of lateral confinement in QWRs are illustrated by the open symbols in Fig. 3(a), calculated by assuming a width to thickness ratio $r_t=0.3$. The anisotropy of the e-hh and of the e-lh transitions reverses sign in comparison with the QW. The dependence of the anisotropy on the ratio r_t is displayed in Fig. 3(b). Note that the curves practically coincide for well thicknesses above 10 nm, where the interaction with the spin-orbit split states becomes negligible. The curves change sign for a ratio $r_t\sim 0.2$, independently of the well thickness. This strong dependence of δ on r_t makes the anisotropy a sensitive probe of the lateral confinement dimensions in QWR structures.

III. EXPERIMENT

The properties of the samples used in the photoluminescence experiments are summarized in Table I. Both samples consist of an array of wires. For sample A, the lateral period is very large, and individual wires can be accessed in microscopic measurements. Sample B contains a vertical stack of three wires with 500 nm pitch. Both samples also contain unstructured regions (denoted well regions), where the lumi-

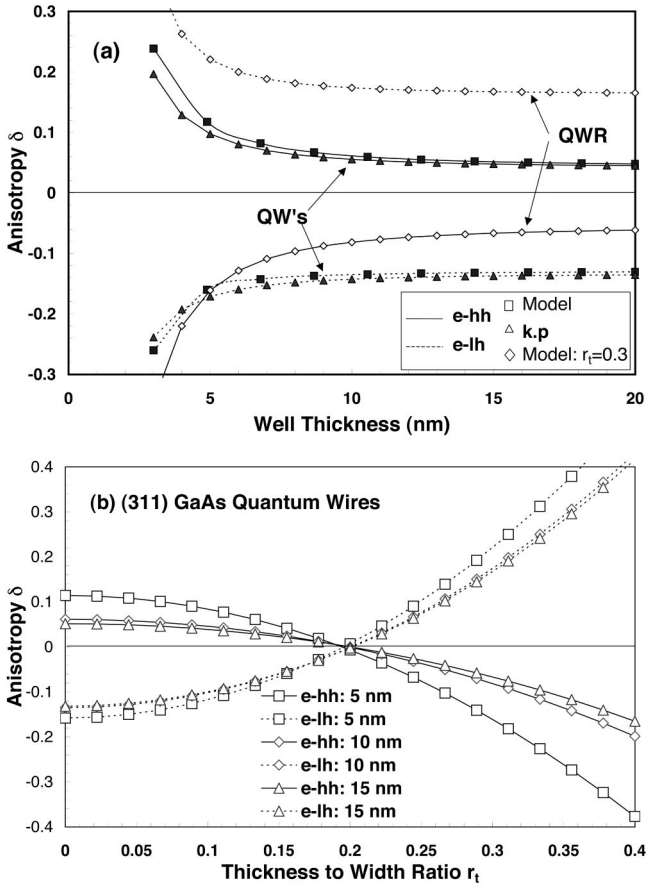

FIG. 3. Calculated optical anisotropy of the e-hh (solid lines) and of the e-lh transitions (dashed lines) of (311)-oriented QW (filled symbols) and QWR (open symbols) as a function of the (a) well thickness and (b) of the ratio r_t between the vertical (along [311]) and lateral (along $[\bar{2}33]$) wire dimensions. The squares (for QWs) and the diamonds (for QWRs) in (a) and the data in (b) were calculated using the model described in the text. The filled triangles in (a) were determined following the $\mathbf{k}\cdot\mathbf{p}$ method from Ref. 18.

TABLE I. Properties of the (311)-oriented wire samples used in this study. The quoted thicknesses were estimated from transmission electron microscopy micrographs (for details see Refs. 3 and 4). The barriers are formed by 50-nm-thick $Al_{0.5}Ga_{0.5}As$ layers.

Sample	Structure	Well thicknesses	Lateral period	Wire thickness	Wire width
A	GaAs/(AlGa)As	6 nm	160 μm	12–13 nm	50 nm
B	3×(GaAs/(AlGa)As)	3 nm	0.5 μm	6 nm	40–50 nm

nescence of the QW can be accessed. Additional details about the structure and the fabrication process are reported in Refs. 3 and 4.

Since the lateral dimension of the wires (cf. Table I) are relatively large, the polarization anisotropy introduced by the lateral confinement is expected to be small. In addition, the detection of the optical anisotropy of a single wire (as for sample A) requires a measurement technique with high spatial and polarization resolution. The experimental setup employed in these studies, illustrated schematically in Fig. 4, is similar to that used in Ref. 19 for microscopic reflection difference (RDS) measurements. The excitation laser beam from a continuous, frequency-doubled Nd vanadate ($Nd:YVO_4$) laser ($\lambda_L = 532$ nm) is spatially filtered (SP), polarized (polarizer P), and then focused by an objective lens (O) onto the sample placed in a cold-finger liquid helium cryostat at 5 K. The spot diameter on the sample surface is $\phi \sim 1\ \mu$m ($\phi \sim 2\ \mu$m), when a 100× (50×) objective is used. The photoluminescence is collected by the same objective and detected by a multichannel spectrometer after passing through a second polarizer (A) and through a confocal spatial filter. The spatial resolution depends on the size of the pinholes placed in the spatial filters and reaches 0.7 μm for pinholes with 100 μm diameter and a 100× objective.

For spatially resolved measurements, the beam splitter (BS) and the objective (O) are scanned in the x–y plane using a special mirror arrangement driven by piezoelectric actuators. This scan mechanism, with a lateral position resolution of 0.05 μm, ensures that the light beam trajectory always coincides with the axis of the objective, thus minimizing polarization distortions during the scan. In addition, the measurement setup possesses an imaging system (not shown in Fig. 4) employing a charge coupled device (CCD) camera to visualize the sample surface. This system is very helpful to localize single wires on the sample surface. For this purpose, the laser beam is initially placed close to the edges of the mesa, which appear as faint lines on the surface image. The precise wire position can then be found by using the scan mechanism to move the beam laterally in order to maximize the wire photoluminescence.

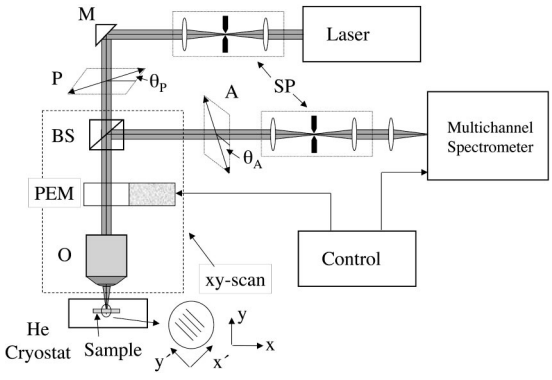

FIG. 4. Scheme of the experimental setup for microscopic anisotropy measurements. The abbreviations have the following meaning, A: analyzer, BS: beam splitter, M: mirror, O: objective lens, P: polarizer, PEM: photoelastic modulator, and SP: spatial filter.

The polarization-sensitive measurements were performed by including a photoelastic modulator (PEM) in the optical path.[9] In these measurements, the sample optical axes x' and y' are aligned halfway between the x and y axes, and the analyzer angle θ_A is set optically parallel to the sample axis y'. The input polarizer P is set along one of the PEM optical axes ($\theta_P = 0°$) to assure that the input beam remains unmodulated by the PEM. The modulator introduces a phase retardation $\delta M = \delta_0 \cos \omega_M t$ ($\omega_M = 50$ kHz is the modulator frequency) between the components of the PL emitted along the x and y directions. In anisotropic samples this phase modulation leads to an intensity modulation after the analyzer A. If $I_{PL,x'} = (I_{PL} + \Delta_{PL})/2$ and $I_{PL,y'} = (I_{PL} - \Delta_{PL})/2$ denote the emitted PL intensity along the x' and y' directions, respectively, the output signal I_d after the analyzer becomes

$$I_d = \tfrac{1}{4}[(1 + a_{BS}^2) I_{PL} + 2 a_{BS} \Delta_{PL} \cos \delta_M], \tag{3.1}$$

where a_{BS} gives the ratio of the beam splitter BS transmission coefficients for polarizations along x and y. The $\cos(\delta_M)$ term can be expanded in terms of Bessel functions as: $\cos(\delta_M) = J_0(\delta_0) + J_2(\delta_0)\cos(2\omega_M) + \cdots$.

The PL anisotropy can be determined with high sensitivity by detecting the second harmonic component of I_d with a lock-in amplifier,[9] following the procedure normally used in RDS. Such a procedure requires a fast detector operating at $2\omega_M = 100$ kHz. In order to keep the advantages of multichannel detection using a CCD camera, we opted instead for the detection of the dc component of I_d as a function of the PEM retardation. By recalling that $J_0(0) = 1$ and $J_0(2.40\ \text{rad}) = 0$, the PL anisotropy $\Delta_{PL} = I_{PL,x'} - I_{PL,y'}$ becomes

$$\Delta_{PL} = \frac{1 + a_{BS}^2}{a_{BS}} \frac{I_d(\delta_0 = 2.40\ \text{rad}) - I_d(\delta_0 = 0\ \text{rad})}{I_d(\delta_0 = 2.40\ \text{rad})} I_{PL}, \tag{3.2}$$

where the prefactor $(1 + a_{BS}^2)/a_{BS} = 2$ for 50% beam splitters.[20]

The change in the detector intensity I_d induced by the modulation of the PEM retardation is a factor of 2 smaller than that obtained, when the analyzer angle is switched between $+45°$ and $-45°$. The former procedure, however, has several advantages for spectroscopic measurements: (i) it is

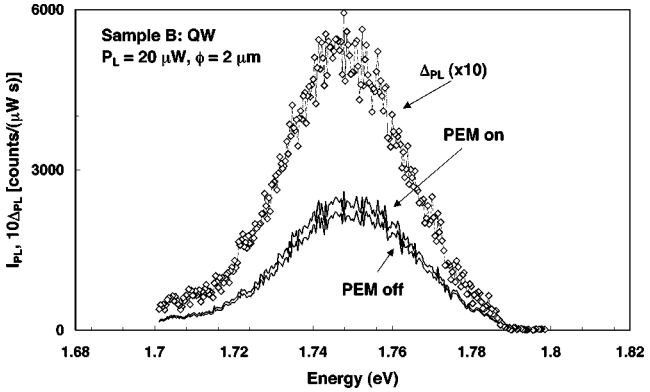

FIG. 5. PL spectra of sample B (in the wire region) recorded with modulator *on* and *off* (lines). The trace with symbols (diamonds) shows the PL anisotropy $\Delta_{PL}=I_{PL,[\bar{2}33]}-I_{PL,[0\bar{1}\bar{1}]}$ corresponding to the difference between the emission polarized along the $[\bar{2}33]$ and $[0\bar{1}\bar{1}]$ directions.

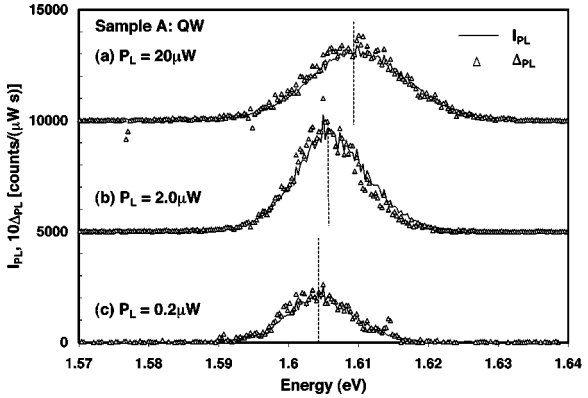

FIG. 6. PL (solid line) and Δ_{PL} (symbols, scaled by a factor of 10) spectra recorded in the well region of sample A using excitation intensities of (a) 20 μW, (b) 2.0 μW, and (c) 0.2 μW. Taking into account the diameter of the excitation spot ($\phi\sim 1$ μm), the corresponding power densities are 3000, 300, and 30 W/cm^2. The curves are shifted vertically for clarity.

fast, since it can be combined with multichannel detection, (ii) can be easily automated, and (iii) does not require moving parts in the optical system. The last point becomes important if high quality crystal polarizers are used, since these can shift the light beams laterally. Finally, the same setup can also be used for PL excitation measurements by setting $\theta_P=45°$ and $\theta_M=0°$ and recording the PL intensity as a function of the incoming laser energy.

The signal-to-noise ratio in the anisotropy measurements is basically determined by the multichannel accumulation time. For measurements with high spatial resolution (such as on single wires), the position stability of the laser spot on the sample surface becomes an important issue. In order to minimize the errors in the anisotropy introduced by position drifts, the measurements were performed by repeating accumulation sequences of the form (PEM on, PEM off, PEM off, PEM on) with relatively short single accumulation steps (1–10 s). Using this procedure, which compensates for slow position drifts, the errors in the anisotropy Δ_{PL}/I_{PL} can be kept below ± 0.01.

IV. RESULTS

A typical example of the PL anisotropy determined using the procedure described in Sec. III is illustrated in Fig. 5. The solid lines display PL spectra of the e-hh transition of sample B recorded in the well region. The lower and upper solid curves were measured with the modulator *off* and *on* (i.e., with a retardation of 2.40 rad), respectively. In the measurements (and through the rest of the article), the $x'=[\bar{2}33]$ and the $y'=[0\bar{1}\bar{1}]$ axes of the samples were aligned as indicated in Fig. 4 with the y' axis parallel to the transmission axis of the analyzer. According to the discussion in Sec. III, the spectra recorded with the modulator *off* and *on* correspond, respectively, to the PL intensity polarized along $y'\|[0\bar{1}\bar{1}]$ and to the average PL intensity, $I_{PL}/2$. For a preferential PL polarization along the $x'\|[\bar{2}33]$ direction, as expected for the e-hh transition in (311)-oriented QWs (cf. Fig. 3), the PL should increase when the modulator is turned on, in agreement with the results in Fig. 5. The trace with symbols in this figure shows the difference $\Delta_{PL}=I_{PL,[\bar{2}33]}-I_{PL,[0\bar{1}\bar{1}]}$ (scaled by a factor of 10). Following Eq. (3.2), the latter is simply given by the difference between the two solid curves multiplied by a factor of 2.

The PL lines of the thin QWs of sample B (Fig. 5) are inhomogeneously broadened with a full width at half maximum (FWHM) of ~ 30 meV. The Δ_{PL} line shape follows closely that of the average PL intensity. This behavior, typical for the well region of the samples, indicates that the anisotropy Δ_{PL}/I_{PL} is essentially the same for all components of the PL line. The anisotropy, therefore, is not affected by extrinsic effects such as recombination through defects. An additional evidence for this intrinsic character of the anisotropy is found in its dependence on the excitation intensity, as illustrated for single wires of sample A in Fig. 6. Due to the small size of the laser spot on the sample surface in the microscopic PL measurements, a blueshift and a broadening of the PL line due to band filling effects is observed even for relatively low (ten's of μW) excitation powers. In all cases, however, Δ_{PL} remains proportional to the PL intensity.

PL spectra recorded with the laser spot placed on different positions on the wires of samples A and B are displayed

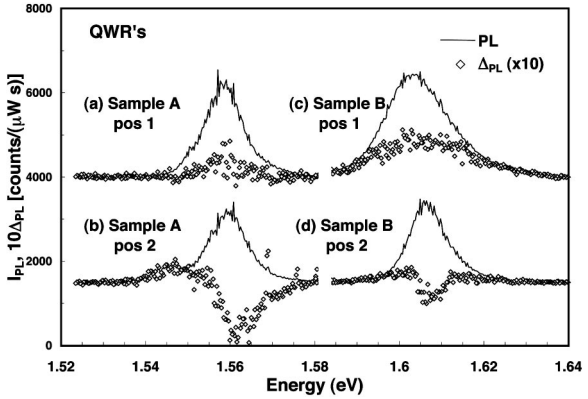

FIG. 7. PL (solid line) and Δ_{PL} (symbols, scaled by a factor of 10) spectra recorded at different positions in the wire region of (a), (b) sample A and (c), (d) sample B.

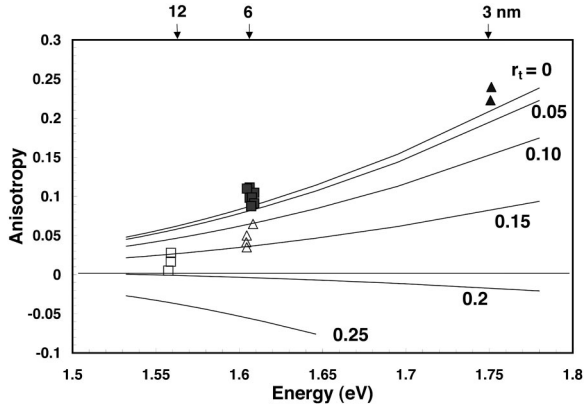

FIG. 8. Average anisotropy of the e-hh transition in QWs (filled symbols) and QWRs (open symbol) as a function of the transition energy measured in samples A (squares) and B (triangles). The lines show the anisotropy calculated with the model described in the text for QWs and for QWRs using the indicated thickness to width ratios r_t.

in Figs. 7(a) and 7(b) and 7(c) and 7(d), respectively. The width of the PL line from the wires is comparable to that for wells with the same thickness. While the PL energy and anisotropy remain relatively constant over the well region, the PL from the wires shows small energy shifts (some meV's), and its anisotropy may vary considerably with position, as indicated in Fig. 7. In some positions the line shape of Δ_{PL} closely resembles that of the PL line, as found for the QWs [see Figs. 7(a) and 7(c)]. However, the anisotropy $\Delta_{\mathrm{PL}}/\mathrm{PL}$ is considerably smaller than that found in the well region, even when the transition energy is the same [compare, for instance, Figs. 7(c) and 6]. We checked that this behavior is independent of the excitation power. As will be discussed in the next section, the reduction and the change in sign of the anisotropy of the wires are attributed to lateral confinement effects.

In other positions, the Δ_{PL} line shape differs considerably from that of the average PL line. These deviations are attributed to potential fluctuations within the microscopic measurement spot, which affect the effective width of the wire. Note that in some cases [Figs. 7(b) and 7(d)] the anisotropy reverses sign, thus indicating a preferential PL emission with polarization parallel to the wires.

In order to compare the anisotropy of the well and of the wire regions, we define the average anisotropy of the e-hh transition as the ratio between the area of the Δ_{PL} and the PL lines. The average anisotropy, measured on different positions on the samples, is plotted as a function of the transition energy for wells (filled symbols) and for wires (empty symbols) in Fig. 8. We included in Fig. 8 only results from PL measurements on wires, where the line shape of Δ_{PL} resembles that of the PL line. In this way, the influence of wire width fluctuations within the illuminated spot on the average anisotropy is minimized. The scattering in the anisotropy data for wires is comparable to that found in QWs. This scattering is mostly due to experimental errors (estimated to be on the order of ± 0.01) in the determination of the absolute anisotropy. Note again the much smaller wire anisotropy as that of the QWs. The experimental data in Fig. 8 will now be compared with the theoretical models of Sec. II.

V. DISCUSSION

The results of the previous section indicate that the PL anisotropy of the wires is considerably smaller and, in some cases, has a sign opposite to that of the (311)-oriented QWs. The reduction in the anisotropy could be attributed to an enhanced recombination through defect centers with isotropic emission properties. Several experimental findings contradict this hypothesis. First, a reduced anisotropy is found even when the Δ_{PL} line shape resembles that of the average PL intensity, thus indicating that the anisotropic emission centers are the same as those responsible for the main component of the luminescence. Second, the anisotropy does not depend on the excitation intensity, as would be expected for defect recombination. Finally, in some positions on the wires, the anisotropy actually changes sign, thus contradicting the initial hypothesis of isotropic emission centers.

Based on the previous arguments, we then attribute the anisotropy reduction (and reversal in sign) to the lateral quantum confinement, which tends to polarize the e-hh transition in the direction parallel to the wires [cf. Fig. 3(b)]. In order to extract information about the lateral confinement dimensions, we compare the average anisotropy plotted in Fig. 8 with the single electron model of Sec. II. The lines display the anisotropy calculated for different ratios $r_t = d_z/d_x$ as a function of the energy of the e-hh transition energy. The relationship between transition energies and well (or wire) thickness required in the calculations was obtained from the measured e-hh transition energies for different well thicknesses. This procedure is justified by the fact that the energy shifts due to the weak lateral confinement present in our samples are negligible compared to those associated with the vertical confinement.

The anisotropy calculated for the QWs slightly underestimates (by $\sim 10\%$) the measured values (filled symbols for $r_t = 0$ in Fig. 8). The effect may be due to an additional contribution from the natural corrugation along the $[\bar{2}33]$ found in (311)-oriented QWs.[21,22] The wire anisotropy for samples A and B fall around $r_t = 0.17 \pm 0.02$ and $r_t = 0.15 \pm 0.1$, respectively, yielding effective wire widths of 70 and 40 nm. The scattering in the experimental data leads to a 10% uncertainty in the effective widths. The effective wire widths determined from the anisotropy agree reasonably well with the values estimated from transmission electron micrographs (cf. Table I). The smaller average thickness for the thinner QWR in sample B is consistent with a higher lateral confinement barrier. In fact, the lateral excitonic confinement barriers, estimated from the difference between the well and wire PL energies, increase from 45 meV in sample A to over 150 meV in sample B.

The effective wire widths discussed above were determined in regions of the sample where the luminescence response is homogeneous over the illuminated spot. In other positions, the luminescence line shape differs considerably from that of the anisotropy [cf. Fig. 7(b) and 7(d)] indicating fluctuations in the wire width within the detection area. These fluctuations are attributed to variations of the as-etched mesa heights, which are known to influence the wire shape,[23] rather than to the growth mechanism that leads to

the sidewall wire formation. In some points, the widths become sufficiently small so as to reverse the sign of the anisotropy, as illustrated in Figs. 7(b) and 7(d). This result clearly demonstrates that the sidewall growth process can produce wires with widths considerably smaller than the values determined above. Note that anisotropy is much more sensitive to the fluctuations in the wire width than the PL energy. The contribution from the lateral confinement to the PL energy in samples A and B, estimated to be of approx. 2.2 and 5 meV for samples A and B, respectively, is smaller than the PL linewidth. As a result, small variations in wire width, which can lead to large changes in the anisotropy, leave the PL line basically unchanged.

VI. CONCLUSIONS

The polarization anisotropy of the photoluminescence from quasiplanar wires fabricated on the (311)A GaAs surface was investigated using an experimental technique that combines a high spatial resolution ($\sim 1\ \mu$m) with a polarization sensitivity below 1%. This technique allows the precise determination of the polarization anisotropy of single wires. We demonstrate that the contribution to the anisotropy from the lateral confinement in the wires opposes that from the vertical confinement. As a result, the anisotropy initially reduces and then reverses signs with increasing lateral confinement. This dependence of the anisotropy is well described by a theoretical model. From a comparison of the model with the experimental data, lateral confinement dimensions between 40 and 60 nm were estimated. These dimensions compare well with those determined by electron transmission microscopy. Finally, the results presented here demonstrate that the sidewall growth process can produce narrow (i.e., with width to thickness ratios inferior to five) and quasiplanar quantum wires.

ACKNOWLEDGMENTS

The authors thank L. Däweritz and H. Grahn for discussions and for a careful reading of the manuscript. They also thank B. Koopmans (Technical University of Einhoven, Netherlands) for many discussions about the experimental setup and acknowledge the expertise of D. Böhme (Max-Planck-Institut für Festkörperforschung, Stuttgart) in the design of the optical table for the microscopic measurements.

[1] L. Pfeiffer, K. W. West, H. L. Stormer, J. P. Eisenstein, K. W. Baldwin, D. Gerschoni, and J. Spector, Appl. Phys. Lett. **56**, 1697 (1990).
[2] E. Kapon, D. M. Huang, and R. Bhat, Phys. Rev. Lett. **63**, 430 (1989).
[3] R. Nötzel, M. Ramsteiner, J. Menniger, A. Trampert, H.-P. Schönherr, L. Däweritz, and K. H. Ploog, Jpn. J. Appl. Phys., Part 2 **35**, L297 (1996).
[4] R. Nötzel, U. Jahn, Z. C. Niu, A. Trampert, J. Fricke, and H.-P. Schönherr, Appl. Phys. Lett. **72**, 2002 (1998).
[5] R. Nötzel, M. Ramsteiner, J. Menniger, A. Trampert, H.-P. Schönherr, L. Däweritz, and K. H. Ploog, J. Appl. Phys. **80**, 4108 (1996).
[6] A. Richter, G. Behme, M. Süptitz, Ch. Lienau, T. Elsaesser, M. Ramsteiner, R. Nötzel, and K. H. Ploog, Phys. Rev. Lett. **79**, 2145 (1997).
[7] A. Richter, M. Süptitz, D. Heinrich, Ch. Lienau, T. Elsaesser, M. Ramsteiner, R. Nötzel, and K. H. Ploog, Appl. Phys. Lett. **73**, 2176 (1998).
[8] Y. Qian, L. Chen, and Q. Wang, Solid State Commun. **87**, 285 (1993).
[9] M. Wassermeier, H. Weman, M. S. Miller, P. M. Petroff, and J. L. Merz, Appl. Phys. Lett. **71**, 2397 (1992).
[10] H. Akiyama, T. Someya, and H. Sakaki, Phys. Rev. B **53**, R4229 (1996).
[11] F. Vouilloz, D. Y. Oberli, M.-A. Dupertuis, A. Gustafsson, F. Reinhardt, and E. Kapon, Phys. Rev. Lett. **78**, 1580 (1997).
[12] F. Vouilloz, D. Y. Oberli, M.-A. Dupertuis, A. Gustafsson, F. Reinhardt, and E. Kapon, Phys. Rev. B **57**, 12 378 (1998).
[13] E. G. Tsitsishvili, Solid State Commun. **100**, 541 (1996).
[14] P. Yu and M. Cardona, *Fundamentals of Semiconductors: Physics and Materials Properties* (Springer, Heidelberg, 1995).
[15] P. V. Santos (unpublished).
[16] J. N. Schulman and Y.-C. Chang, Phys. Rev. B **31**, 2056 (1985).
[17] P. Vogl, H. Hjalmarson, and J. Dow, J. Phys. Chem. Solids **44**, 365 (1983).
[18] E. G. Tsitsishvili, Phys. Rev. B **52**, 11 172 (1995).
[19] B. Koopmans, B. Richards, P. Santos, K. Eberl, and M. Cardona, Appl. Phys. Lett. **69**, 782 (1996).
[20] This prefactor is relatively insensitive to the beam splitter transmission ratio, a_{BS}. For the used beam splitter with $a_{BS}=0.74$ the prefactor $(=2.09)$ differs from 2 by less than 5%.
[21] R. Nötzel, N. Ledentsov, L. Däweritz, M. Hohenstein, and K. Ploog, Phys. Rev. Lett. **67**, 3812 (1991).
[22] P. V. Santos, A. Cantarero, M. Cardona, R. Nötzel, and K. Ploog, Phys. Rev. B **52**, 1970 (1995).
[23] R. Nötzel, M. Ramsteiner, J. Menniger, A. Trampert, H.-P. Schönherr, L. Däweritz, and K. H. Ploog, in *Proceedings of the 24th International Symposium on Compound Semiconductors, San Diego, 8–11 September 1997*, edited by M. Melloch and M. A. Rheed (IEEE 97 TH 8272, Inst. Phys. Publ., Bristol, 1998), p. 65.